Influence of 3D Multi-layer Welding on Residual Stress of Super-big Diameter Welded Hollow Sphere Joint

Ri Namhyok[1,2*], Chen Zhihua[1], Ri Yongsop[2]

1. School of Civil Engineering Tianjin University, Tianjin 300072, PR of China
2. Department of Mechanics, Kim Il Sung University, Pyongyang, DPR of Korea

*Corresponding Author E-mail: rinamhyok@163.com

Abstract: In this paper the influence of 3 dimension multi-layer welding procedure on the welding residual stress of super-big diameter WHSJ(welded hollow sphere joint) in the large-span structure has been evaluated by finite element method. First, a conception of equivalent state change time in the analysis of welding was newly defined, which is the virtual time of state change, representing the absorbing or abstracting heat during state change process between solid and fluid of welding material. By considering of equivalent state change time in real welding and cooling time, the correctness of the thermal analysis was increased. Next, the simulation of three welding methods including single-layer symmetric welding, multi-layer sequential welding and multi-layer symmetric welding was carried out, which shows that multi-layer symmetric welding not only increases the balance of supporting ability of structure but also decreases the maximum tensile residual stress so that it is better than the other two methods.

Keywords: welded hollow sphere joint; welding residual stress; multi-layer welding; symmetric welding; equivalent state change time; large-span structure; ANSYS

1 Introduce

The residual stress occurring in the welding process of structure is influenced by various factors of the mechanical properties of welding material and master material, geometric properties of the welding object, welding method and procedure and so on, and lots of experimental and theoretical research for prediction of residual stress have been performed.

Teng[1] introduced the algorithm of the analysis for deciding the welding residual stress, on the basis of it, described the residual stress and distortions in T-joint fillet welds. Abid[2] studied on a three dimensional sequentially coupled nonlinear transient thermo-mechanical analysis to investigate the effect of tack weld positions root gap on welding distortions and residual stresses in a pipe-flange join. Krasovskyy[3] presented a fatigue assessment for multi-pass welds based on the simulation of welding process, a post-weld treatment and a cyclic fatigue loading. Temperature evolution during welding and X-ray measured residual stresses were compared with the results of simulation as well as failure behavior after cyclic loading. Deng[4] investigated the influence of solid-state phase transformation on the evolution of residual stress distributions in butt-welded 9Cr-1Mo steel pipes with finite element method and experiment. Effects on welding residual stress of the volumetric change and the yield strength change due to austenite-martensite transformation were investigated by means of numerical analysis. Barsoum[5,6] simulated the residual stress in T-joint fillet welds, on linear elastic fracture mechanics, described the relation between residual stress and fatigue crack growth and proved the result of finite element simulation through 2 dimension X-ray experiment.

But in all of these former researches, the influence of the heat of state change have not been considered. In other words, they are all using the heat source model as the multiplication of current, voltage, welding time and efficience. Over here, the most important problem is how to suppose the efficience, but on many occasions it usally depends on experience, does not have sufficient theoretical basis.

According to the wide application of the large-span structure to the architectural construction, the demand of the joint, the important supporting component, has been continually increasing. There are various kinds of joint of the large-span structure, among them the welded hollow sphere joint has simple shape and benefit to support, so it has been being widely used. The joint stress between the welded hollow sphere and tube span depends on material properties, shape and size of the weld joint, welding method and so on.

The welded hollow sphere is manufactured by heating two thick steel circle plates up to high temperature, pressing and deforming them into half-spheres, and in the last welding them each other. Then welding steel tube spans on this welded hollow sphere, there are produced joints or supports. Of course, there may be produced large residual stress not only in the heat plastic treatment process such as heating and pressing and in the weld process of two half spheres, but also in the weld process of the welded hollow sphere and tube span, and these residual stress influence on the supporting ability, deformation and fatigue life of the large span structure. Especially the residual stress between the sphere and the span plays decisive role in supporting ability.

After the appearance of the welded hollow sphere joint, the estimation of residual stress of the welded hollow sphere joint with comparatively small diameter was a very important problem and has been developed continually. Liu and Chen[7] discovered WHSJ in large-span structure and by using material mechanics method, suggested simple formulas to calculate the supporting ability of WHSJ according to the weld joint type. Zhao[8] predicted the welding residual stress at the joint between the welded hollow sphere and tube span with finite element method and extended it to all joints of whole structure and decided the supporting ability of whole structure. Yuan[9] regarded the estimation of residual stress at the joint between the welded hollow sphere and steel tube as the important research task and predicted the influence of diameter and thickness of sphere and tube, welding procedure and velocity on the temperature field and stress field. Then changed this weld residual stress into the initial stress, analyzed the influence on the static characteristics, stiffness and damage of the structure and proved the reliability of the analysis through the residual stress experiment using punching method.

Most of these former researches are all based on the single layer weld of weld hollow spheres with relatively small diameters. But recently according to the rapid extension of span of the large-span structures, more welded hollow spheres have super-big diameters, so the width and depth of weld joint have been continually increased. After all, 3 dimension multi-layer weld of WHSJ in large-span structure is very imperative and at the moment, the influence of the welding residual stress on the mechanical response of structure has been more and more important than ever. However, as reviewing the former study, in the past research on the estimation of residual stress at the joint between welded hollow sphere and tube span, most research are on the basis of single-layer line weld, but few of research on 3 dimension multi-layer weld and symmetric weld has been described.

The essence of research on the super-big diameter WHSJ is to establish the correct assessment criterion for prediction of quantitative influence of welding residual stress and residual deformation on the supporting ability of the structure and suggest the decisive criterion to estimate the advantage or disadvantage of various welding methods.

This paper newly considered the influence of the heat of state change during the welding process and estimated the quantitative effect of 3 dimension multi-layer welding process on welding residual stress of WHSJ with super-big diameter in large-span structure.

2 Theoretical principle

This research treats the residual stress of the joint between the welded hollow steel sphere, whose outer diameter 30cm and thickness is 3cm, and the steel cylinder tube, whose outer diameter is 9cm, thickness is 1.5cm and length is 1.5m. The study ignores the influence of residual stress produced in former manufacturing process of heat plastic treatment and weld of two half spheres. And preheat and temper before and after welding of joint are not performed.

2.1 Thermal transformation process and temperature field analysis

The welding process can be simplified as a nonlinear transient heat transfer process, and welding heat transfer equation and boundary condition can be computed according to Eq.1, 2.

$$\rho(T)c(T)\frac{\partial T}{\partial t}=\frac{\partial}{\partial x}\left(k_x(T)\frac{\partial T}{\partial t}\right)+\frac{\partial}{\partial y}\left(k_y(T)\frac{\partial T}{\partial t}\right)+\frac{\partial}{\partial z}\left(k_z(T)\frac{\partial T}{\partial t}\right)+Q$$

(1)

$$k_n \frac{\partial T}{\partial n} + \bar{q} + h(T - T_0) + \sigma\varsigma(T^4 - T_0^4) = 0 \qquad (2)$$

Where, T_0 is welding temperature(℃), $k_x(T)$, $k_y(T)$, $k_z(T)$ are coefficients of heat conduction in every direction (W/(m·℃)), $\rho(T)$is density(kg/m^3), $C(T)$ is specific heat(J/(kg·℃)), Q is heat source(J/(m^3 s)), k_n is coefficient of heat conduction on boundary(W/(m·℃)), n is distance in normal direction of isothermal surface, $\bar{q}$ is heat flow density on boundary (J/(m^2 s)), ς is emissivity of the surface of the body (ranging from 0 to 1), h is convective heat transfer coefficient of the surface of the body(W/(m^2·℃)), and σ is Stefan–Boltzmann constant which is taken as 5.67×10-8W/(m^2·℃4).

From Eq.1, 2 the thermal equivalent equation of every element is derived as below.

$$\rho\int_{vol} c\{N\}\{N\}^T dv\{\dot{T}_e\} + \rho\int_{vol} c\{N\}\{v_m\}^T [B] dv\{T_e\}$$
$$+ \rho\int_{vol} [B]^T [D][B] dv\{T_e\} = \int_{S_1} \{N\} q^* d(S_1) +$$
$$+ \int_{S_2} T_B h_f \{N\} d(S_2) - \int_{S_2} h_f \{N\}\{N\}^T \{T_e\} d(S_2)$$

(3)

Where, vol is volume of element (m^3), $\{N\}$ is shape function, q^* is heat flow, $\{T_e\}$ is temperature vector of element, S_1 is area of heat conduct(m^2), S_2 is area of convection and heat radiation (m^2), h_f is coefficient of heat film(J/(m^2 s·℃)), $\dot{q}$ is heat generation rate per unit volume (W/(m^3 s)).

Eq.3 may be rewritten as

$$[C_e^T]\{\dot{T}_e\} + ([K_e^{tm}] + [K_e^{tb}] + [K_e^{tc}])\{T_e\} = \{Q_e^f\} + \{Q_e^c\} + \{Q_e^g\} \qquad (4)$$

Where, $[C_e^T]$: element specific heat (thermal damping) matrix, $[K_e^{tm}]$: element mass transport conductivity matrix, $[K_e^{tb}]$: element diffusion conductivity matrix, $[K_e^{tc}]$: element convection surface conductivity matrix, $\{Q_e^f\}$: element mass flux vector, $\{Q_e^c\}$: element convection surface heat flow vector, $\{Q_e^g\}$: element heat generation load. From above formula, temperature according to time and position can be calculated and from the decided temperature, can be calculated thermal deformation.

2.2 Stress Analysis from thermal deformation

The governing equation in thermoelastic deformation

$$\{\sigma\} = [D]\{\varepsilon\} - \{\beta\}\Delta T \qquad (5)$$

$$Q = T_0\{\beta\}^T\{\varepsilon\} + \rho C_v \Delta T \qquad (6)$$

Where, $\{\sigma\}$ is stress vector, $[D]$ is elastic stiffness matrix, $\{\varepsilon\}$ is strain vector, $\{\beta\} = [D]\{\alpha\}$is vector of thermoelastic coefficients, $\{\alpha\}$ is vector of coefficients of thermal expansion, $\Delta T = T - T_{REF}$: subtract of temperatures, T : current temperature, T_{REF} : reference temperature, Q : heat density, $T_0 = T_{REF} + 273K$: absolute reference temperature, C_v : specific heat at constant strain or volume.

Considering Eq.1 and Eq.7:

$$\frac{\partial Q}{\partial t} = T_0\{\beta\}^T \frac{\partial\{\varepsilon\}}{\partial t} + \rho C_v \frac{\partial(\Delta T)}{\partial t} - [K^T]\nabla^2 T \qquad (7)$$

Where, $[K^T]$: thermal conductivity matrix.

Applying the variation principle to stress equation of motion and the heat flow conservation equation coupled by the thermoelastic constitutive equations, produces the following finite element matrix equation:

$$\begin{bmatrix}[M] & 0\\ 0 & 0\end{bmatrix}\begin{Bmatrix}\{\ddot{u}\}\\ \{\ddot{T}\}\end{Bmatrix} + \begin{bmatrix}[C] & [0]\\ [C^{tu}] & [C^t]\end{bmatrix}\begin{Bmatrix}\{\dot{u}\}\\ \{\dot{T}\}\end{Bmatrix} +$$
$$\begin{bmatrix}[K] & [K^{ut}]\\ [0] & [K^t]\end{bmatrix}\begin{Bmatrix}\{u\}\\ \{T\}\end{Bmatrix} = \begin{Bmatrix}\{F\}\\ \{Q\}\end{Bmatrix} \qquad (8)$$

Where, $[M]$: element mass matrix, $[C]$: element damping matrix, $[K]$: element stiffness matrix, $[C^t]$: element specific heat matrix, $[K^t]$: element diffusion conductivity matrix, $[C^{tu}]$: element elastic damping matrix, $[K^{ut}]$: element elastic stiffness matrix.

Thermoplastic strain equation can be produced by considering plastic deformation heat on the thermoelastic strain equation.

$$\begin{bmatrix}[M] & 0\\ 0 & 0\end{bmatrix}\begin{Bmatrix}\{\ddot{u}\}\\ \{\ddot{T}\}\end{Bmatrix}+\begin{bmatrix}[C] & [0]\\ [0] & [C^t]\end{bmatrix}\begin{Bmatrix}\{\dot{u}\}\\ \{\dot{T}\}\end{Bmatrix}+$$
$$\begin{bmatrix}[K] & [0]\\ [0] & [K^t]\end{bmatrix}\begin{Bmatrix}\{u\}\\ \{T\}\end{Bmatrix}=\begin{Bmatrix}\{F\}\\ \{Q\}+\{Q^p\}\end{Bmatrix} \quad (9)$$

Where, $\{Q^p\}=\int_{vol}\dot{Q}_n^p\{N\}dv$,

$\dot{Q}_n^p$ is heat generation velocity of plastic strain per unit volume on nth load step and $\{N\}$ is shape function. From above formula, temperature according to time and position can be calculated.

3 Simulation analysis of welding process

3.1 Physical property of material

In welding process, matrices and weld materials are heated up to much higher temperature than fusing point and during this period, there are produced not only heat deformation but also state change of solid-fluid-solid in the weld material, at last large residual stress is produced. The material of considering welded hollow sphere and tube span is general Q235, its yield strength at ordinary temperature is 235MPa and the grade of weld material is D802（C 0.7-1.44 Si≤2 Mn≤2 Cr 25-32 Fe≤4 W 3-6 other≤4 remainder Co), its yield strength at ordinary temperature is 450MPa.

The thermal and structural properties depend on temperature and they are shown as Fig.1 and Fig.2.

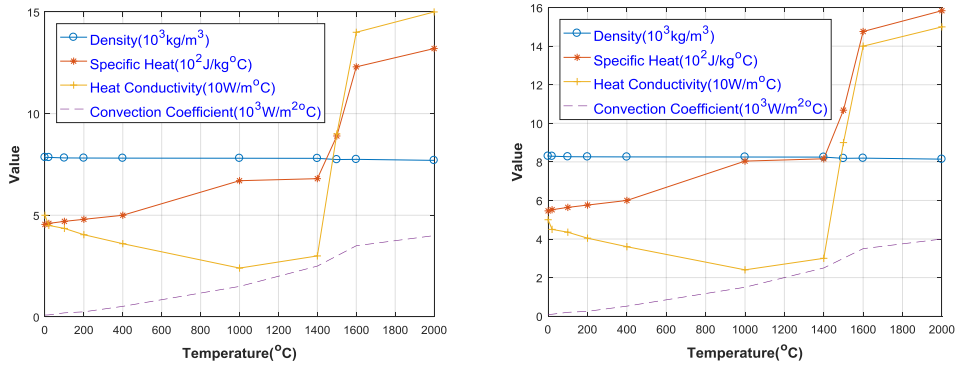

Fig. 1 The thermal properties change according to temperature (matrices, weld material)

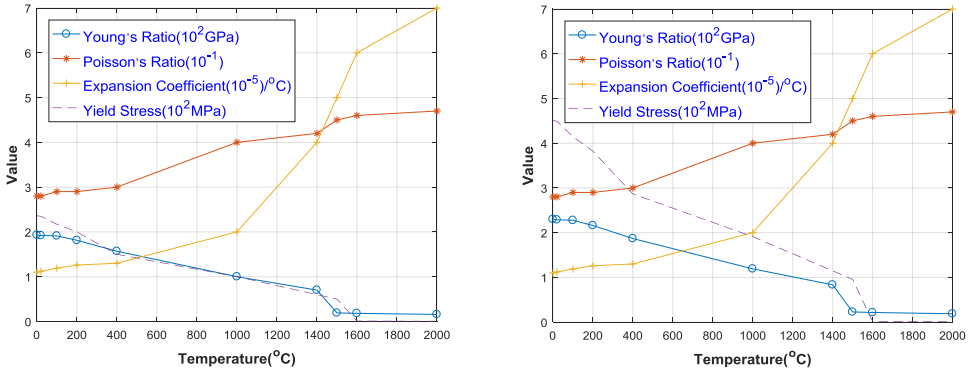

Fig. 2 The structural properties change according to temperature (matrices, weld material)

As shown by Fig.1 and Fig.2, material properties suddenly jump at the boundary of fusing point because at that moment, material state changes from solid to liquid.

3.2 Welding heat load and boundary condition

3.2.1 Heat load considering equivalent state change time

Model of heat source is one of the most important input parameter in numerical thermal analysis. On the 1st law of thermodynamics, during welding process, the heat that matrices and weld material absorb is

$$Q=\eta\int_{t_{wr}}uidt \quad (10)$$

Where, η is efficiency, u,i is voltage and current depending on time, t_{wr} is real welding time. Now consider the numerical range of η. Q is the heat

that matrices and weld material absorb, so it must not be smaller than the heat that weld material absorbs. Of course, among it, the heat that weld material absorbs occupies the most part of Q and it is much more than the heat that is conducted to matrices.

Supposing the considering weld material to be ideal crystal, during the process of state change, the heat transformation cannot produce temperature change, so the temperature of weld material is constant at the fusing point and only the state of material changes, such as melting or solidification process appears. So η must be satisfied

$$\frac{\rho_w V_w\left[\int_{T_{air}}^{T_\lambda} C_s dT + \lambda + \int_{T_\lambda}^{T_{\max}} C_l dT\right]}{\int_{t_{wr}} uidt} < \eta < 1 \qquad (11)$$

Where, C_s, C_l is the specific heat of solid and liquid of weld material depending on temperature, T_{air} is the temperature of ambient air, T_λ is fusing point (1535℃ in this project), $T_{\max}$ is average value of the maximum temperature of weld liquid in every welding sector(in this project, it is supposed to 1910℃), λ is specific melting heat (2.7×10^5J/kg), ρ_w is density of welding material, V_w is sector volume of weld material melted during the welding time.

Supposing the voltage and current are constant during welding process and using the average specific heat in solid and liquid of weld material, then Eq.11 may be simplified as

$$\frac{\rho_w V_w\left[\overline{C_s}(T_\lambda - T_{air}) + \lambda + \overline{C_l}(T_{\max} - T_\lambda)\right]}{UIt_{wr}} < \eta < 1 \qquad (12)$$

Where,

$$\overline{C_s} = \frac{1}{(T_\lambda - T_{air})}\int_{T_{air}}^{T_\lambda} C_s dT,$$

$$\overline{C_l} = \frac{1}{(T_{\max} - T_\lambda)}\int_{T_\lambda}^{T_{\max}} C_l dT$$

They are the average specific heat in solid and liquid of weld material, in this project, they are estimated to 678J/kg℃ and 1512J/kg℃.

Thus substituting voltage and current(U =25v, I =220A), sector volume of weld material melted during the welding time into the Eq.12, the approximate numerical range of η can be decided. In this project, considering that a sector volume is about 5.9×10^{-7}m^3, then the minimum of η is estimated to about 30.1%.

Next, the heat transformation in the change of material state is considered.

The real finite element simulation cannot be reflected the influence of absorbing or emitting heat in change process of state, because there is no temperature change in the melting or solidification process. Therefore, the heat quantity simulated in the melting process is smaller than the actual heat quantity by the heat of fusion, and the heat quantity simulated in the process of cooling is larger than the actual heat quantity by the heat of fusion. On this reason, this paper newly defined a conception of equivalent state change time, by reversing absorption heat or emission heat generated during the change process of state into the equivalent state change time. This equivalent state change time is represneted the time to be subtracted from real welding time in melting process or represented the time to be added to real cooling time in solidification process.

Then the equivalent state change time is calculated.

Supposing that heat transfer velocity is constant in welding process, the equivalent state change time τ_{eq} can be defined as:

$$\tau_{eq} = \frac{\lambda}{\left[\int_{T_{air}}^{T_\lambda} C_s dT + \lambda + \int_{T_\lambda}^{T_{\max}} C_l dT\right]} t_{wr} \qquad (13)$$

Considering Eq.12, then Eq.13 can be rewritten as

$$\tau_{eq} = \frac{\lambda}{\left[\overline{C_s}(T_\lambda - T_{air}) + \lambda + \overline{C_l}(T_{\max} - T_\lambda)\right]} t_{wr} = \eta_m t_{wr} \qquad (14)$$

Where, η_m is the ratio of melting time on the real

weld time. In this project, considering the initial condition and the material properties, the η_m =14.6%. So, the equivalent weld time and equivalent cooling time is

$$\begin{cases} t_{we} = t_{wr} - \tau_{eq} = (1-\eta_m)t_{wr} \\ t_{ce} = t_{cr} + \tau_{eq} = t_{cr} + \eta_m t_{wr} \end{cases} \quad (15)$$

Where, t_{we} is equivalent weld time, t_{ce} is equivalent cooling time, t_{cr} is real cooling time.

After all, the equivalent weld time is about 85.4% of the real weld time and the equivalent cooling time is 1.146 times of real weld time more than the real cooling time. In this project, if the real weld time is 5.3s, real cooling time is 4.2s, the equivalent state change time τ_{eq} is calculated to about 0.8s from Eq.14. Then equivalent weld time is 4.5s, equivalent cooling time is 5s from Eq.15.

3.2.2 Boundary condition

For temperature boundary condition, the opposite end side of tube span against the sphere is constant temperature, the outer surfaces of sphere, span and weld layers are natural convection condition and ambient air temperature is 20℃.

For structure boundary condition, the opposite end side of tube span against the sphere is fixed boundary condition.

3.3 Welding sectors

There are three welding layers including fillet layer and every layer has 12 equal interval welding sectors, so the whole number of welding sectors is 36 and the volume of every sector is the same.Supposed that the voltage and current is constant during welding process, welding volume and time of every sector is divided to the same. (Fig.3)

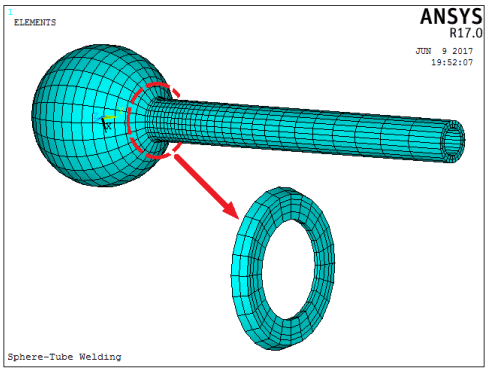

Fig.3 Finite element model of welded hollow sphere joint

3.4 Welding method

The paper uses 3 different welding methods. (Fig.4)

Method 1 is a multi-layer symmetric welding method to perform symmetric weld in the first layer and go on the other layers on this way, method 2 is a multi-layer sequential welding method to perform sequential weld in the first layer and go on the other layers on this way and method 3 is a single-layer symmetric welding method to perform sequential multi-layer weld at one sector and go on symmetric weld at the other sectors. (Fig.4)

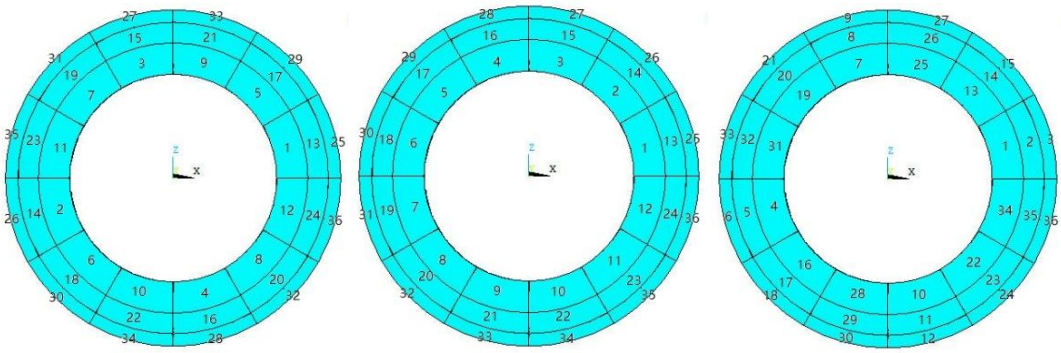

Fig.4 Welding methods

3.5 Welding time

In this project, simulation welding time at one sector is 4.5s, simulation cooling time by natural convection after every welding is 5s, it takes 337s to complete to weld 36 welding sectors. Then cooling time by natural convection after completion of all welds is 4 hours, after all, the entire simulation time is 14742s (4h 5min 42s).

For convergence of solution, the time interval during welding process must be extremely short

(0.001s~0.01s) and for saving the analysis time, the time interval after completion of welding is adjusted to about 10s.

4 Analysis result

4.1 Analysis result of temperature field

On welding method 1, the maximum temperature of weld joint is 1685.9℃ (Fig.5) at the moment of completion of weld (337s) and is 25.7246℃ after cooling 4h by natural convection(14742s), so the temperature approaches to the ambient air temperature (Fig.6).

On welding method 2 and method 3, the maximum temperature of weld joint is similar with on method 1 at the moment of completion of weld (337s) and is 25.7726℃, 25.7585℃ after the same cooling time (14742s).

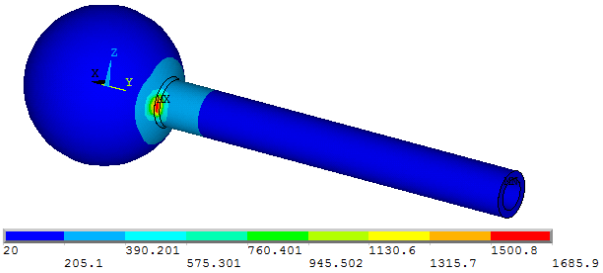

Fig.5 Temperature distribution at the moment of completion of weld (337s)

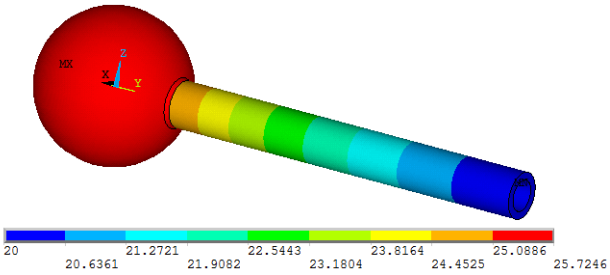

Fig.6 Temperature distribution after cooling 4 hours by natural convection (14742s)

In welding process, the time, position and temperature that the temperature increases up to the maximum value are different from every welding method. On method 1, it is 1968.96℃ in the 11th sector on the first layer at 99.5s, on method 2, it is 2032.13℃ in the 12th sector on the first floor at 109s and on method 3, it is 2073.96℃ in the 32nd sector on the third floor at 299s.(Fig.7)

This shows that the maximum temperature is the lowest on multi-layer symmetric weld among three welding methods. In the figure, unlinked partitions are sectors that has not been yet welded.

Then the temperature changes at the center of the first sector on the first layer according to welding time (0~400s) are considered. (Fig.8)

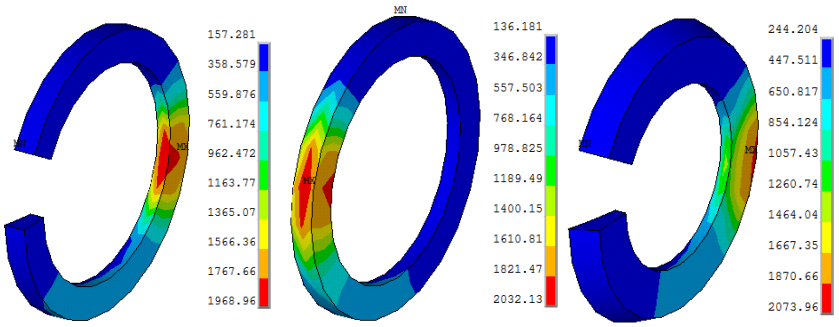

Fig.7 Maximum temperature and position according to welding methods

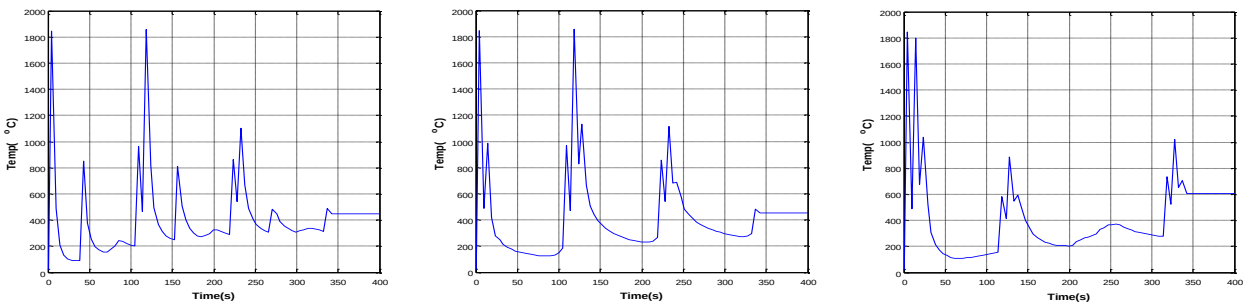

Fig.8 Temperature change according to time

Three graphs show that the temperature change at the surveying point in the first welding sector has difference from every welding method. On method 1, in whole welding time, the temperature increases three times up to about 1820℃, 1820℃, 1120℃ at every interval time of one layer welding time(114s) and in one layer welding time, the temperature increases twice, when welding the neighbor sectors, up to about 850℃, 980℃ by influence of symmetric welding. On method 2, in whole welding time, the temperature increases three times up to about 1820℃, 1820℃, 1120℃ at every interval time of one layer welding time (114s) as method 1, but in one layer welding time, the temperature slowly decreases in the former half part of the layer and increases again in the next half part of the layer by influence of sequential welding. On method 3, in whole welding time, the temperature increases three times, when welding own sector and the neighbor sectors, up to about 1820℃, 870℃, 1030℃ by influence of symmetric welding.(Fig.8)

4.2 Analysis result of stress field

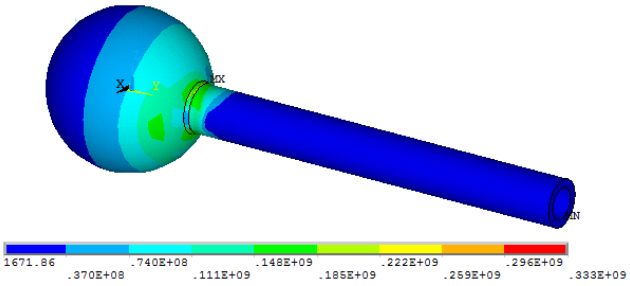

Fig.9 Von-Mises stress distribution at the last moment of welding (337s)

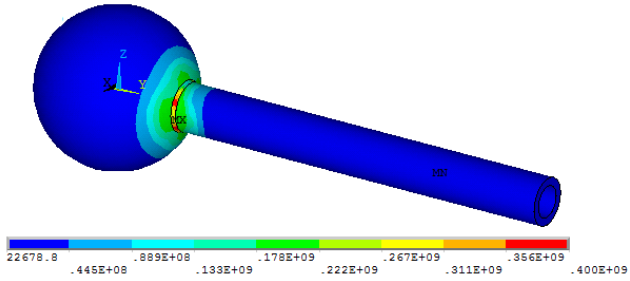

Fig.10 Von-Mises stress distribution after 4 hours of cooling by natural convection (14742s)

On welding method 1, von-Mises stress distribution at the last moment of welding (337s, max 333MPa) and after 4 hours of cooling by natural convection (14742s, max 400MPa) are shown by Fig.9, 10.

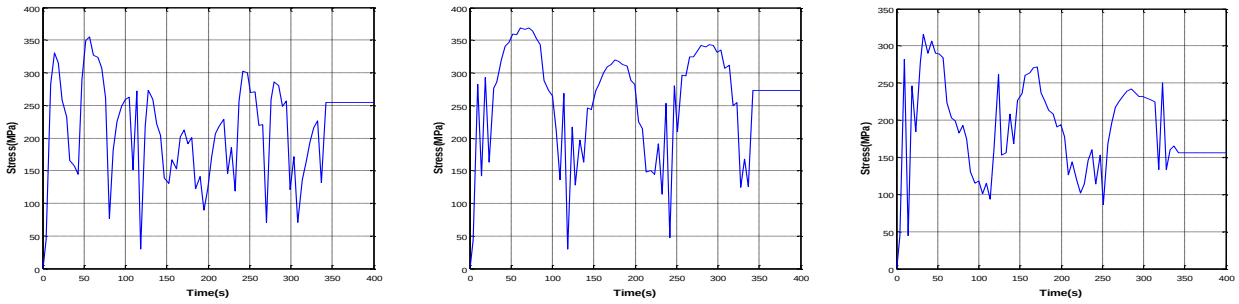

Fig.11 Von-Mises stress change according to time

The von-Mises stress change at the center of the first sector on the first layer according to welding time (0~400s) is shown by Fig.11.

These graphs show that the stress at surveying point on every method increases up to 350~380MPa and thoroughly depends on the temperature change graphs. The stress decreases every when the temperature increases by welding and increases every when the temperature decreases by cooling, the local maximum stress points on stress change graph (Fig.11) becomes the local minimum temperature points on temperature change graph. (Fig.8) In other words, the type of stress graph is upside-down to the temperature graph.

Then the residual stress at welding material after 4 hours of cooling (14742s) is discribed more detailed.

Firstly, von-Mises residual stress is described.

On every method the maximum von-Mises residual stresses all approaches to the yield strength of weld material, but the distribution is different from each method.(Fig.12)

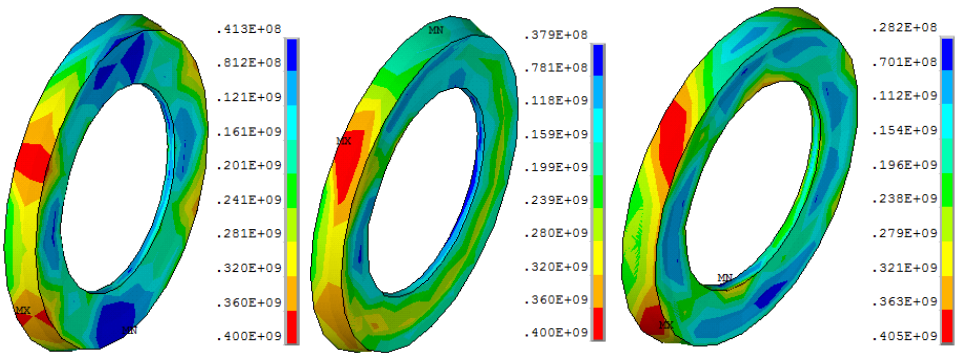

Fig.12 Von-Mises residual stress distribution according to welding method

On method 1 and method 3, residual stress distribution is symmetric on the link axis of sphere and span, but on method 2, the residual stress distribution is asymmetric and high stresses are concentrated at the location beginning weld, decreases along the weld route. So on method 2, nevertheless to say, supporting ability of structure will be unbalanced.

Next, principle residual stress vector and principle tensile residual stress are described.

On every method, the location of maximum tensile stress is the outer surface of upper layer on the angle of direction of the first welding sector from the center of the weld cylinder ring. The residual stress distribution, on method 1 and method 3, consists of 4 tension-compression partitions and the value of maximum tensile stress on method 3 is 1.36 times, 140MPa higher than on method 1. On method 2, the stress state slowly decreases from tensile to compress along the welding floor direction. (Fig.13, 14)

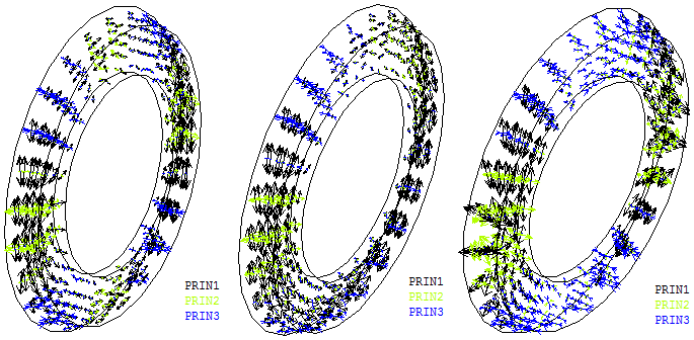

Fig.13 Principle residual stress vector according to welding method

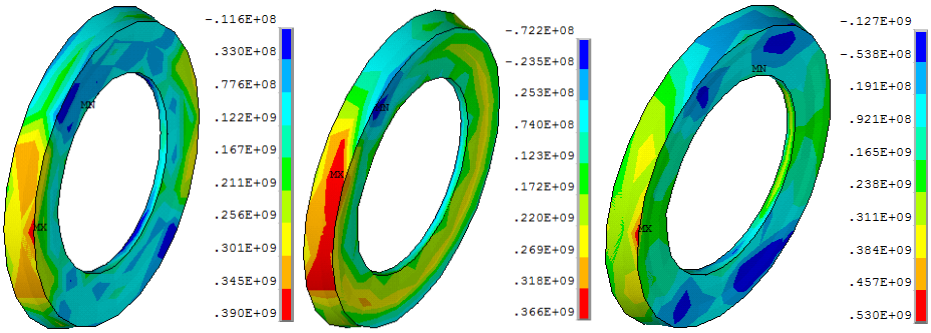

Fig.14 Principle tensile residual stress distribution according to welding method

Finally, the component residual stresses are described.

For considering the change of stress according to positions, three paths are set up.(Fig.15)

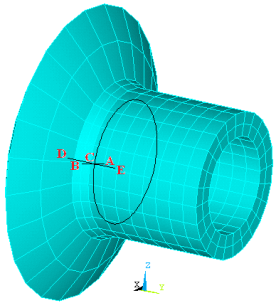

Fig.15 Considering Paths

The first path AB is the radial direction linear path passing through the center of the first welding sector, where A is a point at the bottom of the first welding sector in the first floor,B is a point on the outer surface of the same sector in the third floor. The second path is the hoop direction circular path passing C, where C is the center of second sector in the second floor and rotating direction is welding direction on method 2. The last third path DE is the axial direction linear path passing through C, where D is in the welded hollow sphere and E is a point in the circular tube (Fig.15).

Radial stress distribution and graphs of component stresses on radial direction path AB are shown in Fig.16, 17. Radial stress distribution is similar with other stress distributions, but absolute value is smallest of three component stresses. Graphs of component stresses on the path explain that from A to B on the path, stress values increase on method 1 and 2, decrease on method 3.

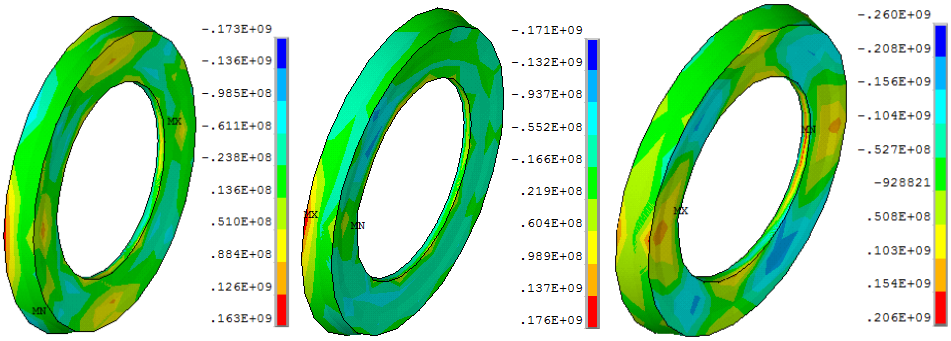

Fig.16 Radial residual stress distribution according to welding method

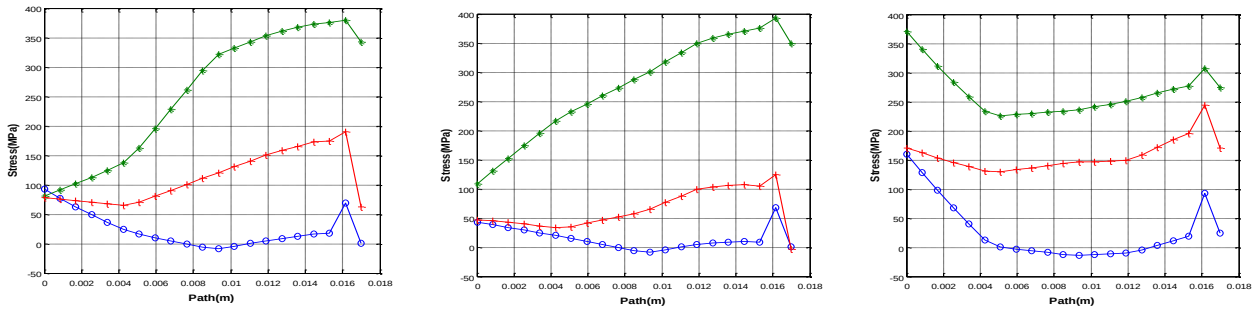

Fig.17 Graphs of component stresses on radial direction path AB (-o: radial stress, -*: hoop stress, -+: axial stress)

Hoop stress distribution and graphs of component stresses on hoop direction path C are shown in Fig. 18, 19. Hoop stress distribution is similar with von-Mises stress distribution, but absolute value is smaller than it. Graphs of component stresses on the path explain that on the circular path, on method 1 and method 3, there are repeated 4 partitions of tension-compression and the difference of every peak value on method 1 is smaller than that on method 3, and on method 2, the stress slowly decreases along the weld direction.

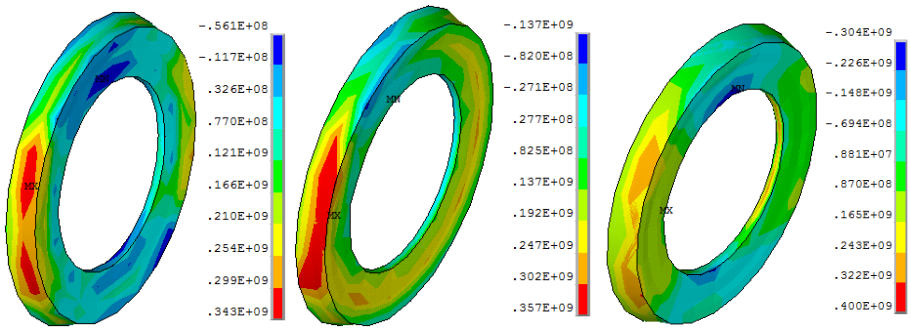

Fig.18 Hoop residual stress distribution according to welding method

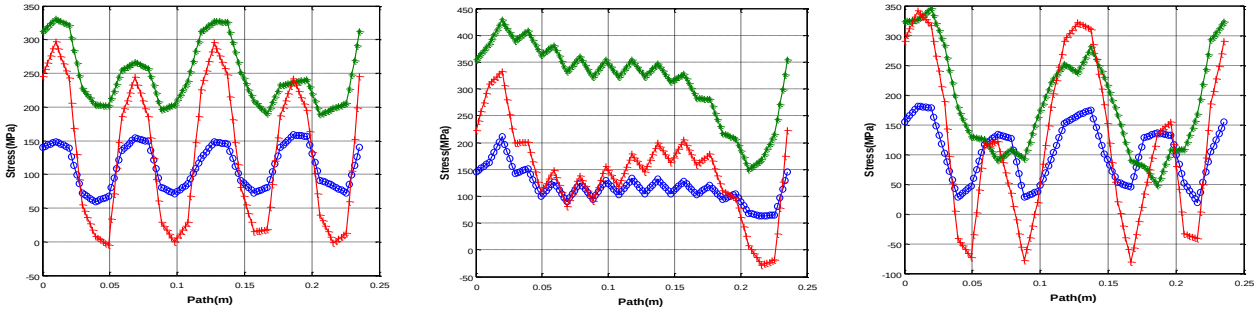

Fig.19 Graphs of component stresses on hoop direction path C (-o: radial stress, -*: hoop stress, -+: axial stress)

Axial stress distribution and graphs of component stresses on axial direction path from D to E are shown in Fig.20, 21. Axial stress distribution is similar with hoop distributions, but stress size on method 3 is largest of them. Graphs of component stresses on the path explain that stress sizes in weld material are largest, in the linked part of the circular tube nearby the welding part are smallest.

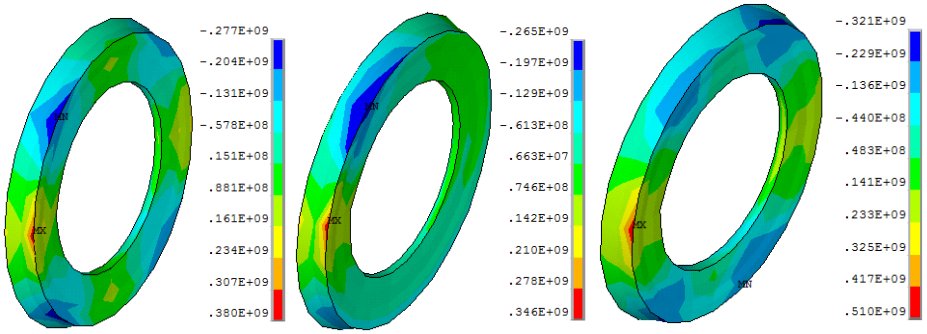

Fig.20 Axial residual stress distribution according to welding method

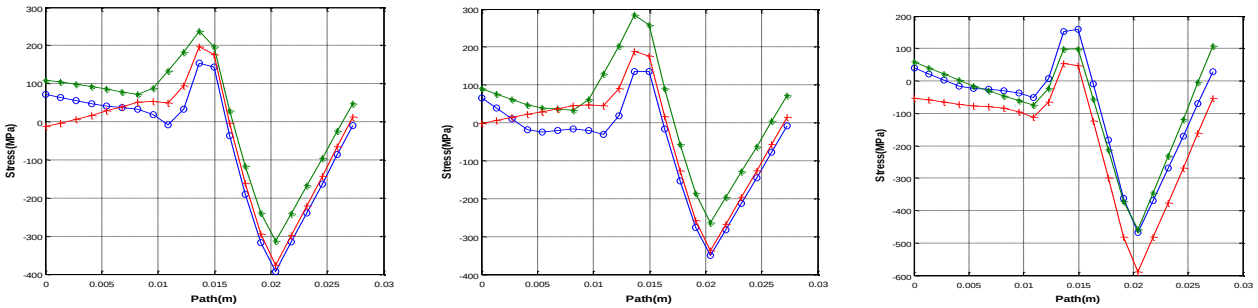

Fig.21 Graphs of component stresses on axial direction path DE (-o: radial stress, -*: hoop stress, -+: axial stress)

After all, on every method, among three component stresses, the axial stress and hoop stress play important role and influence of the radial stress is the smallest. Stress distribution is also symmetric on method 1 and method 3 and asymmetric on method 2, stress value on method 3 is much higher than on method 1. On method 3, radial stress is 1.26 times (46MPa), hoop stress is 1.17 times (57MPa) and axial

stress is 1.34times (130MPa) higher than those on method1, so it means that on the multi-layer symmetric welding method, the radial stress, the hoop stress and the axial stress are smaller than on the single layer symmetric welding method by 79.3%, 85.4% and 74.6%, respectively.

5 Conclusions

Based on the results of the study, the following conclusions can be made.

1) When analyzing the welding process with the finite element method, considering the effects of melting and solidification processes, the heat for the material state change during the simulation process must be subtracted from the actual welding heat and added to the actual cooling heat. The amount of heat for this change in melting or solidification can be simulated by reversing the absorption or emission heat generated during the state change process to an equivalent state change time.
2) The equivalent state change time is 14.6% of the actual welding time. From this, the simulation time in the melting process becomes smaller than the actual welding time by the equivalent state change time, and the simulation time in the solidification process becomes larger than the actual cooling time by the equivalent state change time.
3) The residual stress distribution and its value, produced during 3 dimension multi-layer welding process of super-big welded hollow sphere joint in large-span structure, are much different from various welding methods. On every method, the location of maximum tensile stress is the outer surface of upper layer on the angle direction of beginning weld from the center of the weld cylinder ring. Among three component stresses, the axial stress and hoop stress play important role and influence of the radial stress is the smallest.
4) The multi-layer symmetric welding method is more balanced than the multi-layer sequential welding method, and the radial stress, the hoop stress and the axial stress are smaller than the single layer symmetric welding method by 79.3%, 85.4% and 74.6%, respectively.

References

[1]Teng T L, Fung C P, Chang P H, et al. Analysis of residual stresses and distortions in T-joint fillet welds[J]. International Journal of Pressure Vessels and Piping, 2001, 78(8): 523-538.

[2]Abid M, Siddique M. Numerical simulation to study the effect of tack welds and root gap on welding deformations and residual stresses of a pipe-flange joint[J]. International Journal of Pressure Vessels and Piping, 2005, 82(11): 860-871.

[3]Krasovskyy A, Sönnichsen S, Bachmann D. On the residual stresses in multi-pass welds: coupling of welding simulation and fatigue analysis[J]. Procedia Engineering, 2011, 10: 506-511.

[4]Deng D, Murakawa H. Prediction of welding residual stress in multi-pass butt-welded modified 9Cr–1Mo steel pipe considering phase transformation effects[J]. Computational Materials Science, 2006, 37(3): 209-219.

[5]Barsoum Z, Barsoum I. Residual stress effects on fatigue life of welded structures using LEFM[J]. Engineering failure analysis, 2009, 16(1): 449-467.

[6]Barsoum Z, Lundbäck A. Simplified FE welding simulation of fillet welds–3D effects on the formation residual stresses[J]. Engineering Failure Analysis, 2009, 16(7): 2281-2289.

[7] Liu Xiliang, Chen Zhihua. Link of the welded hollow sphere joint and cylinder tube in spatial truss structure[J]. Steel Structure,1991,4:52-54.

[8]Zhao Zhong-Wei, Zhu Han , Chen Zhi-Hua, Mechanical behavior of single-layer reticulated shell connected by welded hollow spherical joints with considering welding residual stress[J]. Weld World (2016) 60:61–69

[9] Yuan Zhijun. A study on numerical simulation of weld of cylinder tube and the influence factor of welding residual stress[D].Nanchang University,2010.